

Comparative assessment of renewable energy-based hydrogen production methods

H. Ishaq^{*}, I. Dincer

Clean Energy Research Laboratory (CERL), Faculty of Engineering and Applied Science, University of Ontario Institute of Technology, 2000 Simcoe Street North, Oshawa, Ontario, L1H 7K4, Canada



ARTICLE INFO

Keywords:

Biomass
Solar
Geothermal
Renewable hydrogen: sustainability
Energy
Efficiency

ABSTRACT

Hydrogen is acknowledged as a potential fuel as it can be used as an energy carrier, a storage medium, in fuel cells and as a fuel as well and offers carbon-free solutions. This paper investigates three renewable energy based configurations for hydrogen production. The renewable energy sources considered in this study are solar PV, geothermal power generation and biomass gasification. The proposed study also presents a novel configuration of biomass gasification for hydrogen production via multistage water gas shift reactors. The solar PV and geothermal energy based hydrogen production systems are analysed employing the EES software while the hydrogen production system employing biomass gasification is simulated employing Aspen Plus. All three designed configurations are proceeded through numerous parametric analyses to investigate the system behavior and effect on system efficiencies. The hydrogen production using biomass gasification technique provides with the energetic and exergetic efficiencies of 53.6% and 49.8% and the efficiencies for the geothermal power generation based hydrogen production system are found to be 10.4% and 10.2% respectively. The exergetic and energetic efficiencies of hydrogen production system employing solar PV system are found to be 17.45% and 16.95%, respectively and the system is designed to produce 1.13 mol/s of hydrogen. Furthermore, the results of the parametric studies and sensitivity analyses are presented and discussed.

1. Introduction

One of the major challenges is to address the growing global energy demand and to figure out the ways to meet this demand by sustainable and environmentally-benign energy solutions [1]. The continuous upsurge in the population and living standards give rise to the global energy demand [2]. At present, the major part is set to be supplied by fossil fuel supplies but these materials are geographically restricted [3]. Fossil fuels carry the disadvantage of faster depletion and greenhouse gas emissions. Because of the limited supplies, fossil fuels are not projected to meet the cumulative demand and more researches are being conducted on renewable energy systems [4]. Hydrogen is acknowledged as a potential fuel as it can be used as an energy carrier, a storage medium, in fuel cells and as fuel and it offers carbon-free solutions [5]. Generally, when electricity is compared with hydrogen, electricity carries disadvantages of transmission and heat losses caused by high voltages and electrical resistance while hydrogen offers some advantages, such as high effectiveness of energy conversion, abundant sources, aptitude to be created with zero emissions from water, long-distance transportation,

storage options availability, conversion into fuels, the possibility of being produced by renewable energies and eradicate the environmental harm and high -lower and -higher heating values as compared to the traditional fossil fuels [6].

Collier et al. [7] presented a conference paper on a solar energy-based hydrogen production. The solar parabolic concentrating photovoltaic system was considered for the electrical output and it is further connected to the hydrogen producing electrolyzer. The PV cells made of single-crystal silicon were plugged in series-parallel combination to generate 200 A of current at 2–2.5 V for power single cell of the electrolyzer. Jeon and Min [8] conducted a study on the monolithic photovoltaic-electrolytic cell-based hydrogen production. This study considered a new hydrogen production technique of combining an electrolytic cell with photovoltaic and recommended this combination as one of the most promising methods regarding stability and efficiency. Mainly, they focused on the water oxidation electrocatalysts and their methods of fabrication for monolithic PV-electrolytic. Saadi et al. [9] published a study on the solar photovoltaic based hydrogen production in Algeria. They focused on the east region of Algeria named as Biskra, where solar energy is available, for the solar photovoltaic based

* Corresponding author.

E-mail address: haris.ishaq@uoit.net (H. Ishaq).

Nomenclature		<i>Subscripts</i>	<i>Acronyms</i>
A	area (m^2)	ω	moisture content
C	carbon	θ	temperature ratio
\dot{E}_n	energy rate (kW)	β	biomass parameter
ex	specific exergy (kJ/kg)		
F	Faraday's constant		
h	specific enthalpy (kJ/kg)		
H	hydrogen		
HHV	higher heating value (kJ/kg)		
I	direct normal irradiance (kW/m^2)		
J	current density		
k	thermal conductivity ($\text{W}/(\text{m}^2\text{K})$)		
LHV	lower heating value (kJ/kg)		
LHV	molar lower heating value		
\dot{m}	mass flow rate (kg/s)		
\dot{N}	number of moles		
N	nitrogen		
\dot{n}	mole flow		
O	oxygen		
p	partial pressure		
P_{solar}	solar power		
\dot{Q}	heat rate (kW)		
s	specific entropy (kJ/kg K)		
T	temperature ($^\circ\text{C}$)		
V	voltage		
\dot{W}	Power or work rate (kW)		
<i>Greek letters</i>			
η	energy efficiency		
ψ	exergy efficiency		

hydrogen production by PEM electrolyzer. This study considered the three different types of PV generators with 6 kW of rated power followed by the electrolyzer for hydrogen production. The characteristics of the PV panel considered in this study were validated experimentally, and the outcomes achieved by simulation and compared results with experimental data. The prompt solar irradiance and temperature effects were also investigated against PV characteristics and both models were validated as well.

Hosseini and Wahid [10] presented a detailed study on the renewable and sustainable energy-based hydrogen production methods exploring the green energy. This article presented the supercritical water gasification of biomass as one of the best thermochemical processes in terms of cost-effectiveness as moisturized biomass was fed to the gasifier directly without drying process and cost of hydrogen storage was also minimized as hydrogen was produced at high-pressure. The lower efficiencies of the solar source and expensive PV cells were disclosed as the development activities.

Udomsirichakorn and Salam [11] presented a review study on the calcium oxide (CaO) chemical looping based biomass gasification for hydrogen production. Biomass gasification offers a sustainable, feasible and environment-friendly preference for hydrogen production with large-scale higher hydrogen yields to meet the hydrogen needs. They acknowledged CaO as a suitable, cheap and abundant catalyst for biomass-based hydrogen-rich gas production. In order to conquer the deactivation of CaO because of carbonation, the CaO chemical looping gasification (CLG) was reviewed in detail. They first investigated the biomass gasification based hydrogen production without catalysts and then explored the CaO catalyst based biomass gasification for producing and the overlooks and prospects of the biomass gasification accompanied with CaO catalyst based CLG were deliberated as an auspicious process for sustainable, renewable and environment-friendly production

of hydrogen. Iribareen et al. [12] conducted a study on the lignocellulosic biomass gasification based hydrogen production and presented the exergetic and environmental evaluation. In the life cycle assessment (LCA), seven potential impacts were considered namely; global warming, cumulative energy demand, ozone layer depletion, land competition, photochemical oxidant formation eutrophication and acidification. The life-cycle energy balance of the system suggests a relatively promising energy performance. In order to improve the energy and environmental performance, some key factors predicted by this study were namely; reducing poplar demand, dropping the demand of natural gas for steam reforming, refining logistical biomass supply planning and electricity demand optimization.

Nikolaidis and Poullikkas [13] present a comprehensive study on the different processes for hydrogen production. This study considered 14 hydrogen production methods and conducted a comprehensive economic, technical comparative analysis. The gasification and pyrolysis (thermochemical) were found economically viable and showed the potential of becoming competitive with conventional methods. Further research was recommended for biological methods for hydrogen production. The sole purpose of this study was to reduce the dependence on the fossil fuels and replace them with clean energy sources.

Sikarwar et al. [14] presented a review study on the advancements in the biomass gasification. This study discussed various comparative conventional methods for biomass gasification and presented the recent advances as well. They also considered and discussed the unique biomass gasifiers accompanied by multi-generation to encourage this multi-generation technology into alternate applications requiring higher flexibility and efficiency. Muresan et al. [15] conducted the techno-economic analysis for different hydrogen production methods using biomass and coal gasification. Ud Din and Zainal [16] conducted a technological overview on the biomass gasification systems integrated

with solid oxide fuel cell (SOFC) systems. This review study comprehended the biomass gasification components, SOFC, biomass characteristics, factors affecting biomass gasification, gasifier undergoing thermochemical conversion, cleaning technologies and different integrations of gasifier and SOFCs.

Yilmaz et al. [17] presented a study on the geothermal energy-based production and liquefaction of hydrogen and conducted the economic analysis. This study proposed seven different configurations for hydrogen production and liquefaction. The major process included in the study were electrolysis, a two-stage geothermal plant and a hydrogen liquefaction cycle (Linde-Hampson). The hydrogen production and liquefaction cost projected by this study were found in the range of 0.979 \$/kg to 2.615 \$/kg of hydrogen. Missimer et al. [18] conducted a study on the geothermal energy-based desalination and electricity production system. They also combined geothermal source with a desalination system where the exhaust stream from the turbine was passed through the multi-effect desalination unit to consume the harvested latent heat. A renewable energy-based electricity generation and desalinated water production system was introduced within the geothermal energy framework.

This study aims at three different approaches for renewable energy-based hydrogen production. The renewable energy sources considered in this study are solar PV, biomass gasification and geothermal energy based hydrogen production. A unique configuration of the biomass gasification based hydrogen production is proposed in this study which is further integrated with multistage water gas shift reactors to achieve higher production. The Aspen Plus industrial software and Engineering equation solver (EES) are used to simulate the presented frameworks. Following are the explicit objectives of the current study: (i) to develop three different configurations for renewable energy-based hydrogen production methods (ii) to analyse all three configurations using energy and exergy approach, (iii) developing a new approach of multi-stage water gas shift reactor (MWGSR) to convert CO in CO_2 and to produce hydrogen and (iv) to investigate the viability and scale-up possibilities using numerous parametric study and sensitivity analyses.

2. System description

This study consists of the three different configurations of renewable energy-based hydrogen production. The energy sources considered in this study are biomass gasification, geothermal and solar PV. Fig. 1 represents the solar PV based hydrogen production, Figs. 2 and 3 show the hydrogen production through biomass gasification and Fig. 4 displays the geothermal energy based hydrogen production system. The Aspen Plus flowsheet for biomass gasification based hydrogen production is represented in Fig. 3. Table 1 represents some of the operating

parameters for all three designed configurations. All three hydrogen production configurations are described in detail in this section.

2.1. Solar photovoltaic power based hydrogen production

The installed solar PV panel absorbs the solar irradiance and produces the electrical power. The number of solar PV panels considered for the analysis is 20, solar irradiance of 800 W m^{-2} is considered during the simulation and the efficiency of solar PV panel is assumed to be 15% [19]. The electricity produced by the solar PV panel is DC and PEM electrolyzer also requires DC power, thus, it is directly fed to the PEM electrolyzer. The PEM electrolyser absorbs the electrical output of the PV panels, operates at 80°C of temperature and 1 bar of pressure and splits water into hydrogen and oxygen.

2.2. Biomass gasification based hydrogen production

The type of biomass used in this study is bamboo wood. The compositions of different components for ultimate and proximate analysis are arranged in Table 1. The biomass gasification reaction B3 is carried out at 850°C temperature and 24.31 bar of pressure to attain high-grade syngas [20]. The chemical composition represents the reactor biomass composition balance. The chemical reactions involving volatile matter combustion reactions and chemical species decomposition from char are written as

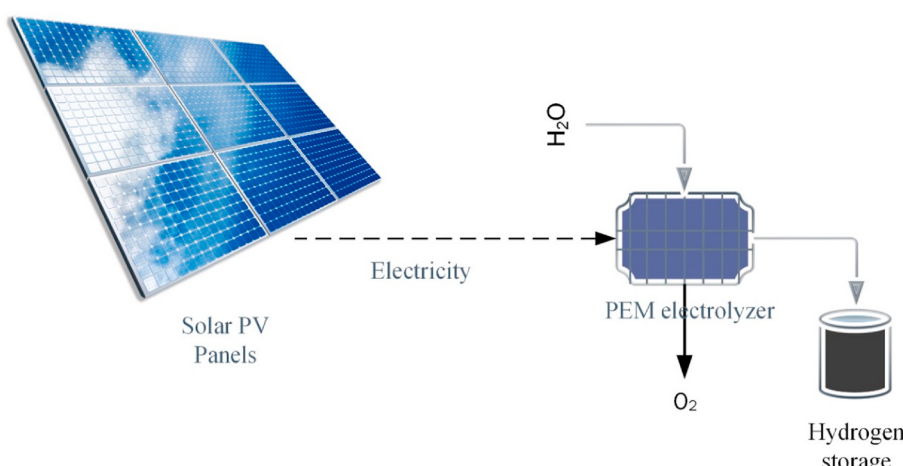
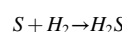
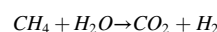
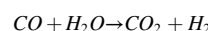
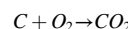
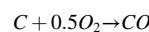
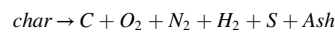
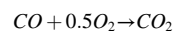
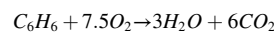
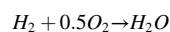
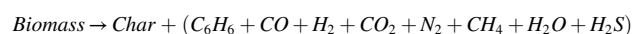


Fig. 1. Solar photovoltaic power source based hydrogen production.

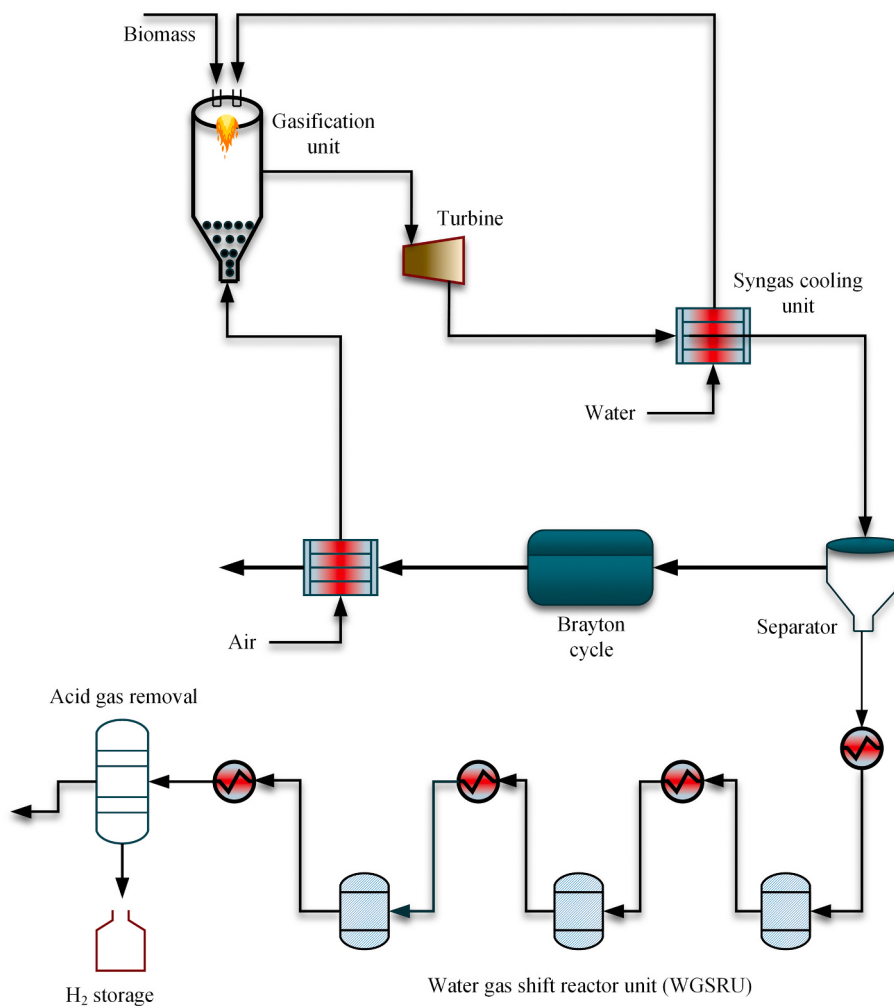
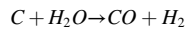


Fig. 2. System schematic of the biomass gasification based hydrogen production configuration.



The syngas then moves to a turbine B4 where high temperature and pressure are used to achieve power and syngas further passes through heat exchanger B1 where syngas is cooled by heating up the input water and converting it into steam. A part of syngas is separated towards the Brayton cycle while remaining leads to the multi-stage water gas shift reactor (MWGSR). The Brayton cycle is used to produce the electricity to meet the work requirement for the compressors and the additional latent heat is utilized by heating oxygen before entering the gasifier. A multistage water gas shift reactor approach is employed within the system which converts CO into CO₂ by reacting it with steam and produces hydrogen gas. The heat exchangers are placed to recover the additional heat and to maintain the reaction temperatures. The produced hydrogen is separated in the next step for industrial applications.

2.3. Geothermal power generation based hydrogen production

The major components of the geothermal power generation based hydrogen production system are production well, turbine, generator, converter, reinjection well and PEM electrolyser. The input temperature for the geothermal fluid is the 240 °C and input pressure is 33.47 bar [21]. The hot geothermal fluid passes through a flash chamber which converts saturated liquid into the saturated mixture and produces vapor. This vapor stream then passes through the turbine to generate electricity. The generator is employed to convert mechanical work into electrical work and converter converts AC in DC currently which is

directly fed to the PEM electrolyser. This electrolyser split water into oxygen and hydrogen. The reaction carried out in the PEM electrolyser is as follows:



3. Analysis and assessment

All three proposed configurations are analysed thermodynamically considering every individual component. The solar PV and geothermal power based systems are analysed and modeled using EES while biomass gasification based configuration is simulated using Aspen Plus under RK-SOAVE property method. The operating parameters and the detailed description of each component are arranged in Table 2. This section undergoes the major model equations used for each component and investigation of the performance index in terms of the overall energetic and exergetic efficiencies.

3.1. Solar PV based system

The designed system consists of two major components of the solar photovoltaic panels and PEM electrolyser. This section governs the concerning model equations used for analysing the mentioned components and overall efficiency equations.

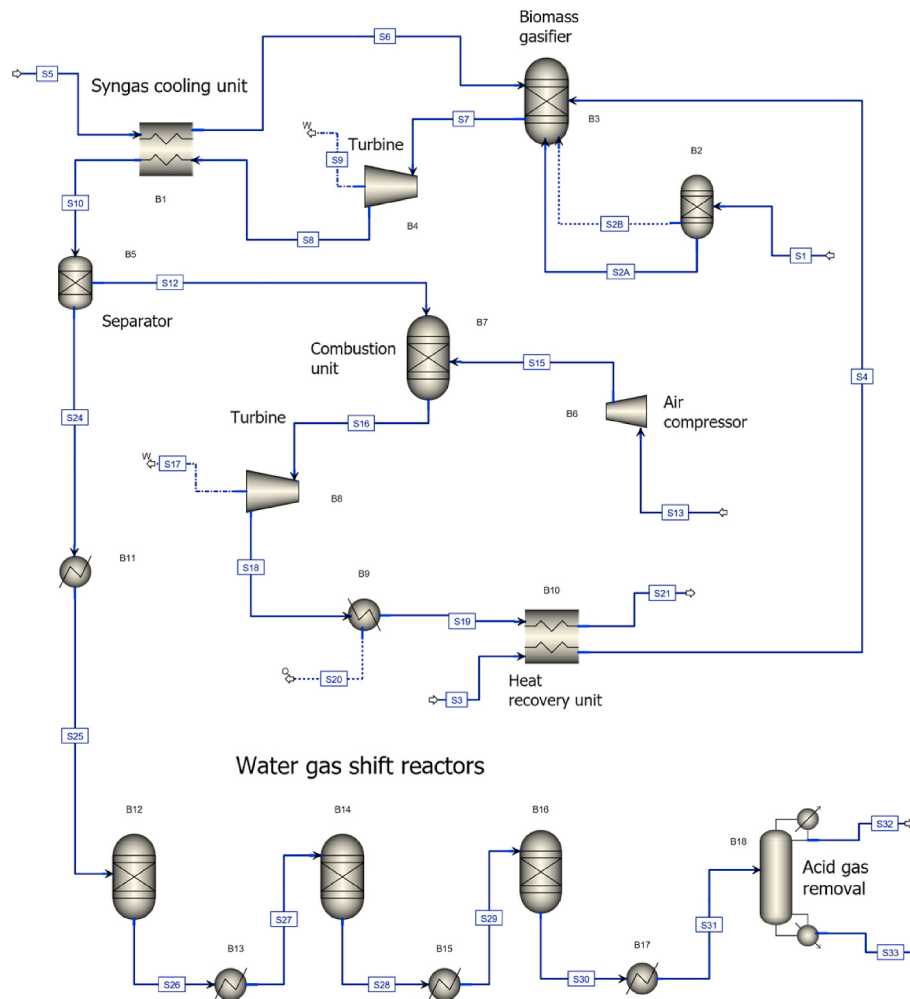


Fig. 3. Biomass gasification based hydrogen production system.

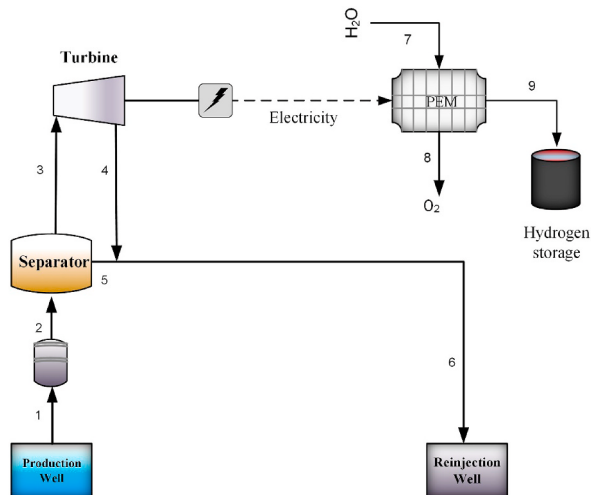


Fig. 4. Geothermal power based hydrogen production configuration.

3.1.1. Solar PV panel

The power produced by the solar PV cells which is further employed to the PEM electrolyser can commonly be expressed as [23]:

$$P_{PV} = I_{solar} \times A_{PV} \times \eta_{PV} \quad (2)$$

Table 1
Biomass composition considered for the designed system [22].

Component	Bamboo wood (% by wt)
Proximate analysis as received	
Moisture	11.50
DAF (dry ash free) volatile matter	86.80
Fixed carbon	11.24
Ash	1.95
Ultimate analysis dry ash free	
C	50.71
H	6.32
O	42.77
N	0.2
HHV	20.574 MJ/kg

Here, I_{solar} is the solar irradiance assumed to be $0.8 \frac{kW}{m^2}$, A_{PV} is the area of the PV panel whose dimensions are assumed to be $10 \times 10 m^2$ and η_{PV} is the solar PV panel efficiency.

3.1.2. Proton exchange membrane electrolyser

The PEM electrolyser is used to split water hydrogen and oxygen using electrical power. In the designed configurations, PEM electrolyser is employed to the solar PV, and the geothermal power generation based hydrogen production systems. In both of these configurations, all of the electric power extracted from solar PV and geothermal power source is employed to the PEM electrolyzer to produce hydrogen. The required energy for the PEM electrolyser is as follows:

Table 2

Component description and specification for all the designed configurations.

Block name	Component type	Description	Component Specification
Solar PV based hydrogen production system	Solar PV panel	Solar photovoltaic panels absorb the solar irradiance and produce electric power	$I_{solar} = 0.8 \frac{kW}{m^2}$ $A_{PV} = 10 \times 10$ $\eta_{PV} = 0.15\%$
	PEM electrolyser	PEM electrolyser utilizes the electric power produced by solar panel for hydrogen production	$T_{elec} = 80^\circ C$ $P_{elec} = 1bar$
Biomass gasification based hydrogen production system	Heat exchanger (B1)	Syngas cooling unit using counter current heat exchanger used to supply steam to the gasifier	Steam output temperature = 423.52 °C Counter current heat exchanger
	Gasifier (B3)	Gasifier used for biomass gasification using oxygen and steam	Operating pressure = 24.31 bar Operating temperature = 850 °C
	Turbine (B4)	Expands the high-temperature gasifier output to generate power	Discharge pressure = 0.5 bar Isentropic efficiency = 0.72%
Geothermal power based hydrogen production system	Compressor (B6)	Recovers the additional amount of heat available which is used for heating	Discharge pressure = 28 bar Discharge temperature = 648 °C
	Turbine (B8)	Expands the high-temperature combusted gas to generate power	Discharge pressure = 0.1 bar Isentropic efficiency = 0.72%
	Heat exchanger (B10)	Counter current heat exchanger used to recover the heat for heating oxygen	Oxygen output temperature = 496 °C Counter current heat exchanger
	Water gas shift reactor B12, B14 and B16	Water gas shift reactor used to convert CO into CO ₂ using steam and produces hydrogen	Operating pressure = 14.4 bar Operating temperature = 450 °C
	Flash chamber	Flash chamber is employed to improve the steam quality and lowers the pressure as well	Flashing pressure = 6 bar Flashing temperature = 240 °C
	Turbine	Expands the input coming from the flash chamber and generates the electricity which is further converted in DC for PEM electrolyser	Turbine inlet pressure = 6 bar Turbine outlet temperature = 1.5 bar
	PEM electrolyser	PEM electrolyser utilizes the electric power produced by geothermal power generation system for hydrogen production	$T_{elec} = 80^\circ C$ $P_{elec} = 1bar$

$$\Delta H = \Delta G + T\Delta S \quad (3)$$

Here, ΔG signifies Gibbs function and $T \Delta S$ denotes thermal energy.

The PEM electrolyser hydrogen production rate can be expressed as the following correlation [24]:

$$\dot{N}_{H_2} = \frac{J_{el}}{2F} \quad (4)$$

Here, F symbolizes Faraday's constant, \dot{N}_{H_2} denotes the mole flow of hydrogen and J_{el} signifies current density. The expression for the excess electricity that is electrical energy input rate employed to the electrolyzer is represented as:

$$\dot{W}_{PEM} = J_{el}V \quad (5)$$

$$V = V_0 + V_{act,a} + V_{act,c} + V_{con,a} + V_{con,c} + V_{Ohmic} \quad (6)$$

Here, V is voltage, V_0 is reversible cell potential which is calculated by Nernst equation [25]:

$$V_0 = \frac{\Delta G}{nF} + \frac{RT}{nF} \ln \left(\frac{(p_{H_2})(p_{O_2})^{0.5}}{p_{H_2O}} \right) \quad (7)$$

The correlations for the activation over-potential and exchange current density are expressed as follows [26]:

$$J_{o,i} = J_i^{ref} \exp \left(\frac{E_{act,i}}{RT} \right) \quad (8)$$

$$V_{act,i} = \left(\frac{RT}{F} \right) \sinh^{-1} \left(\frac{J_{el}}{2J_{o,i}} \right) \quad (9)$$

Here, n is number of electrons, p is partial pressure, i is either cathode or anode, J_i^{ref} is pre-exponential factor and $J_{o,i}$ is exchange current density. The correlation for the Ohmic over-potential is expressed as [26]:

$$V_{Ohmic} = R_{PEM} J_{el} \quad (10)$$

The overall energetic and exergetic efficiencies of the solar PV based hydrogen production system can be expressed as follows:

$$\eta_{SolarPV} = \frac{\dot{m}_{H_2} LHV_{H_2}}{I_{solar} \times A_{PV}} \quad (11)$$

$$\psi_{SolarPV} = \frac{\dot{m}_{H_2} ex_{H_2}}{I_{solar} \times A_{PV} \left(1 - \frac{T_0}{T_{sun}} \right)} \quad (12)$$

3.2. Biomass gasification based system

The nonconventional material of biomass has been added manually using the input data to the Aspen Plus which is employed to the decomposition reactor before the biomass gasifier. Gibbs reactor is employed to the Gibbs reactor to achieve the feasible gasification results. As it can be depicted from Fig. 3, a decomposition reactor is employed for biomass and char decomposition. The biomass composition considered for the designed system is arranged in Table 1. As lower heating value is dependent on the biomass chemical composition, the correlations used to calculate the biomass chemical exergy and biomass parameters β can be expressed as [27]:

$$ex_{ch}^f = [(LHV + \omega h_g) \times \beta + 9.417S] \quad (13)$$

$$\beta = 0.1882 \frac{H}{C} + 0.061 \frac{O}{C} + 0.0404 \frac{N}{C} + 1.0437 \quad (14)$$

Here, ω is moisture content, β is biomass parameter, H is hydrogen, C is carbon, N is nitrogen and O is oxygen. The syngas lower heating value can be calculated by the following expression [28]:

$$LHV_{syngas} = \sum_i \dot{m}_i \times \overline{LHV}_i \quad (15)$$

Here, i is gas constituent, \dot{m} symbolizes mole flow and \overline{LHV}_i represents the molar lower heating value of specific gas constitute. The model equation for the major components of the biomass gasification based hydrogen production system are as follows:

Heat Exchanger B1.

For heat exchanger

$$\dot{m}_{s5}h_{s5} + \dot{m}_{s8}h_{s8} = \dot{m}_{s6}h_{s6} + \dot{m}_{s10}h_{s10} \quad (16)$$

$$\dot{m}_{s5}ex_{s5} + \dot{m}_{s8}ex_{s8} = \dot{m}_{s6}ex_{s6} + \dot{m}_{s10}ex_{s10} + \dot{E}x_d \quad (17)$$

Gasification reactor B3.

For gasifier

$$\dot{m}_{s1}LHV_{s1} + \dot{m}_{s4}h_{s4} + \dot{m}_{s6}h_{s6} - \dot{Q}_{Decomp} = \dot{m}_{s7}h_{s7} \quad (18)$$

$$\dot{m}_{s1}ex_{s1} + \dot{m}_{s4}ex_{s4} + \dot{m}_{s6}ex_{s6} - \dot{Q}_{Decomp} \left(1 - \frac{T_0}{T}\right) = \dot{m}_{s7}ex_{s7} + \dot{E}x_d \quad (19)$$

Turbine B4.

For turbine

$$\dot{m}_{s7}h_{s7} = \dot{m}_{s8}h_{s8} + \dot{W}_{out} \quad (20)$$

$$\dot{m}_{s7}ex_{s7} = \dot{m}_{s8}ex_{s8} + \dot{W}_{out} + \dot{E}x_d \quad (21)$$

Separator B5.

For separator

$$\dot{m}_{s10}h_{s10} = \dot{m}_{s12}h_{s12} + \dot{m}_{s24}h_{s24} \quad (22)$$

$$\dot{m}_{s10}ex_{s10} = \dot{m}_{s12}ex_{s12} + \dot{m}_{s24}ex_{s24} + \dot{E}x_d \quad (23)$$

Compressor B6.

For compressor

$$\dot{m}_{s13}h_{s13} + \dot{W}_{in} = \dot{m}_{s15}h_{s15} \quad (24)$$

$$\dot{m}_{s13}ex_{s13} + \dot{W}_{in} = \dot{m}_{s15}ex_{s15} + \dot{E}x_d \quad (25)$$

Heater B9.

For heater

$$\dot{m}_{s18}h_{s18} = \dot{m}_{s19}h_{s19} + \dot{Q}_{out} \quad (26)$$

$$\dot{m}_{s18}ex_{s18} = \dot{m}_{s19}ex_{s19} + \dot{Q}_{out} \left(1 - \frac{T_0}{T}\right) + \dot{E}x_d \quad (27)$$

Water gas shift reactor B12.

For WGSR

$$\dot{m}_{s25}h_{s25} = \dot{m}_{s26}h_{s26} + \dot{Q}_{out} \quad (28)$$

$$\dot{m}_{s25}ex_{s25} = \dot{m}_{s26}ex_{s26} + \dot{Q}_{out} \left(1 - \frac{T_0}{T}\right) + \dot{E}x_d \quad (29)$$

The overall energetic and exergetic efficiencies of the biomass gasification based hydrogen production system can be expressed as follows:

$$\dot{W}_{net} = \dot{W}_{B4} + \dot{W}_8 - \dot{W}_{B6} \quad (30)$$

$$\eta_{Gasification} = \frac{\dot{m}_{H_2}LHV_{H_2} + \dot{W}_{net}}{\dot{m}_{biomass}LHV_{biomass}} \quad (31)$$

$$\psi_{Gasification} = \frac{\dot{m}_{H_2}ex_{H_2} + \dot{W}_{net}}{\dot{m}_{biomass}ex_{biomass}} \quad (32)$$

3.3. Geothermal power generation based system

The geothermal power generation is considered as the electricity

source for this configuration and the electric power harvested from the geothermal power generation system is directly employed to the PEM electrolyser for hydrogen production, after being converted into DC current. The model equations for the major components of the geothermal power generation based hydrogen production system are given as follows:

Flash chamber.

For flash chamber

$$\dot{m}_1h_1 = \dot{m}_2h_2 \quad (33)$$

$$\dot{m}_1ex_1 = \dot{m}_2ex_2 + \dot{E}x_d \quad (34)$$

Separator.

For separator

$$\dot{m}_2h_2 = \dot{m}_3h_3 + \dot{m}_5h_5 \quad (35)$$

$$\dot{m}_2ex_2 = \dot{m}_3ex_3 + \dot{m}_5ex_5 + \dot{E}x_d \quad (36)$$

Turbine.

For turbine

$$\dot{m}_3h_3 = \dot{W}_T + \dot{m}_4h_4 \quad (37)$$

$$\dot{m}_3ex_3 = \dot{m}_4ex_4 + \dot{W}_T + \dot{E}x_d \quad (38)$$

The efficiency of the generator is assumed to be 80%. Thus, the total electrical output will be the product of mechanical work and generator efficiency [29].

$$\dot{W}_{el} = \eta_{gen} \dot{W}_T \quad (39)$$

The overall energy and exergy efficiencies of the geothermal power generation based hydrogen production system can be written as:

$$\eta_{Geothermal} = \frac{\dot{m}_{H_2}LHV_{H_2}}{\dot{m}_1(h_1 - h_6)} \quad (40)$$

$$\psi_{Geothermal} = \frac{\dot{m}_{H_2}ex_{H_2}}{\dot{m}_1(ex_1 - ex_6)} \quad (41)$$

4. Results and discussion

Several parametric studies and sensitivity analyses for each system and their results are presented in this section.

4.1. Parametric studies and sensitivity analyses for solar PV based system

Solar PV panel based hydrogen production system is one of the three configurations presented in this study. Thus, it is significant to investigate the performance of the solar PV panels and PEM electrolyser

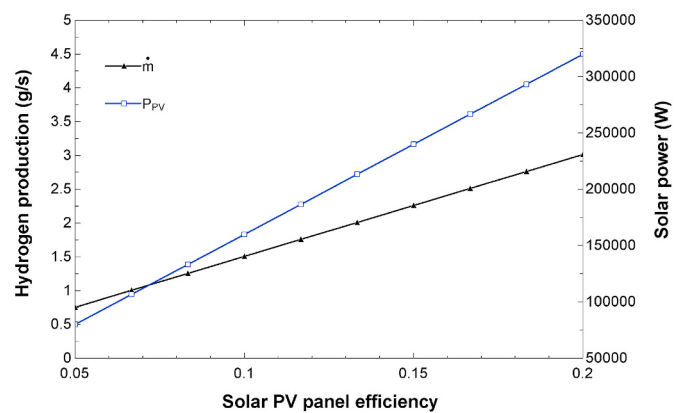


Fig. 5. Solar PV panel efficiency effect on solar power and hydrogen flowrate.

employed with it. Solar PV panels efficiency, solar power, PEM electrolyser performance in terms of hydrogen production, and the efficiencies are the major parameters for this system which need to be investigated. Fig. 5 displays the effect of solar PV panel efficiency on the solar power and hydrogen capacity. The system is designed in a way that generated solar power is supplied to the PEM electrolyser directly. The range of the PV panel efficiency is taken in the range of 0.05–0.2%. With the rise in PV panel efficiency, panel generates more solar power and increased solar power results in higher hydrogen capacity. The symbol \dot{m} represents the mass flowrate of hydrogen in g/s. The effect of solar PV panel efficiency is investigated against the overall energetic and exergetic efficiencies and results are displayed in Fig. 6.

Two different types of symbols are used to represent the energy and exergy efficiencies. The range of the solar PV panel efficiency is taken in the range of 0.05–0.2%. The rise in the solar PV panel efficiencies increases the solar power and increased solar power results in higher hydrogen capacities. It can be depicted from the figure that overall energy and exergy efficiencies rise with the increase in solar PV panel efficiencies.

4.2. Parametric studies and sensitivity analyses for biomass gasification based system

Hydrogen production using the biomass gasification technique is simulated using Aspen Plus industrial software. It is noteworthy to investigate the system in terms of system inputs and output, hydrogen production capacities, heat duties and efficiencies. The biomass gasifier has three input of steam, biomass and oxygen, which plays an important role in the system performance and syngas composition. Fig. 7(a) exhibits the effect of biomass and steam flowrates on the hydrogen production capacities. Biomass enters to the gasifier via stream S1 while water is converted into steam by cooling the syngas and reaches to the gasifier via stream S6. The range of biomass flowrate is taken from 0.1 to 1 kg/s and the steam flowrate is set to increase in intervals of 0.25 kg/s from 0.5 to 2 kg/s. It can be depicted that the hydrogen flow rate increases with the rise in the biomass and steam flowrates.

Fig. 7(b) exhibits the effect of biomass and steam flowrates on the steam fraction in the output stream. The flowrates of biomass and steam are taken in the same ranges. It can be depicted that steam fraction in the output stream increases in the beginning and starts decreasing gradually and oxygen flowrate is kept constant during this sensitivity analysis.

Fig. 7(c) displays the effect of the biomass and steam flowrates on the carbon dioxide flowrate in the syngas. Biomass flowrate is taken on x-axis and carbon dioxide flowrate is plotted on y-axis and intervals of rise in steam flowrate are shown in legends. It can be depicted from the figure that flowrate of CO₂ increases at the beginning for all flowrates of

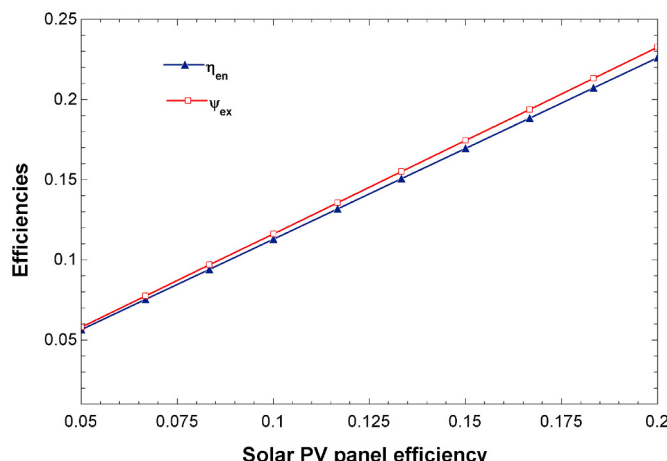


Fig. 6. Effect of solar PV panel efficiency on the energy and exergy efficiencies.

steam with the rise in biomass flowrate but the streams with the lower flowrates of steam show lower mass fraction of CO₂ in syngas which increases gradually for higher steam flowrates. It can be observed that for the higher flowrates of steam, the mass fraction of CO₂ in the syngas rises with the increase in the biomass flowrate.

It is significant to investigate the mass fractions of each component in the syngas leaving the biomass gasification unit. The mass fraction of each syngas constituent namely; nitrogen, carbon dioxide, hydrogen, steam and carbon monoxide is dependent on the flow rates of both input steam and biomass. Fig. 8 (a) and (b) display the effect of steam input flow rate and biomass input flow rate on the mass fractions of the significant components of nitrogen, carbon dioxide, hydrogen, steam and carbon monoxide.

In addition, Fig. 8(a) exhibits the effect of the steam input flow rate on the mass fractions of each component. The input steam flow rate ranged from 0.1 kg/s to 2 kg/s. It is evident that steam mass fraction increases initially and starts decreasing gradually while the mass fraction of carbon dioxide increases throughout with the rise in steam input flow rate. The mass fractions of remaining constituents decrease gradually with increasing steam input flow rate. Fig. 8(b) shows the effect of biomass input flow rate on the mass fractions of each component. The input biomass flow rate ranged from 0.1 kg/s to 2 kg/s. It is evident that carbon dioxide mass fraction increases initially and starts decreasing gradually while the mass fraction of steam decreases throughout and mass fractions of remaining constituents increases gradually with the rise in input biomass flow rate.

The effect of the steam flowrate is investigated against the hydrogen flowrate in Fig. 9. Water enters the heat exchanger via stream S5 which is converted into steam by cooling the syngas and reaches to the gasifier via stream S6. The carbon monoxide present in the syngas is converted to the carbon dioxide by reacting it with steam and producing hydrogen. A series of three reactors are employed for water gas shift reaction which converts CO into CO₂ and raises the amount of hydrogen produced. It can be depicted that hydrogen flowrate goes on the higher level after every reactor and flowrate increases gradually.

Fig. 10(a) displays the effect of oxygen flowrate on the hydrogen capacity in all three reactors. Oxygen reaches to the gasification reactor via stream S4 and it is one of the major input for the gasifier and effect the syngas composition. Stream S26, S28 and S30 are leaving the water gas shift reactors B12, B14 and B16. It can be depicted that the excess of oxygen causes a decrease in the hydrogen flowrate. For all three streams S26, S28 and S30, the amounts of hydrogen is observed to decrease because the amount of biomass and steam are taken as constant and the reaction is dependent on all three input parameters of steam, biomass and oxygen.

The flowrate of oxygen is investigated against the power generated by the turbines B4 and B8 in Fig. 10(b). Syngas passes through turbine B4 where high temperature and pressure are used to generate electrical work and B8 is the Brayton cycle turbine which is also used to generate power. The range of oxygen flowrate is taken from 0.1 to 1 kg/s. It can be depicted that the rise in oxygen flowrate causes the work rate to increases gradually for both turbines. The primary y-axis is presenting the work generated by turbine B8 while the secondary y-axis is showing the power produced by turbine B4.

Fig. 10(c) exhibits the effect of oxygen flowrate on the heat duty of all three water gas shift reactors placed in series. The novel idea of a new configuration for water gas shift reaction is also proposed in this study to achieve the higher conversion rates. Stream S26, S28 and S30 are leaving the water gas shift reactors B12, B14 and B16. The range of oxygen flowrate is taken from 0.1 to 2 kg/s. The water gas shift is an exothermic reaction that evolves the heat during the reaction. This study is significant as it is important to investigate the amounts of heat evolved by the series of reactors. It can be depicted that the rise in oxygen flowrate causes the heat duty to decrease because the amount of biomass and steam are taken as constant.

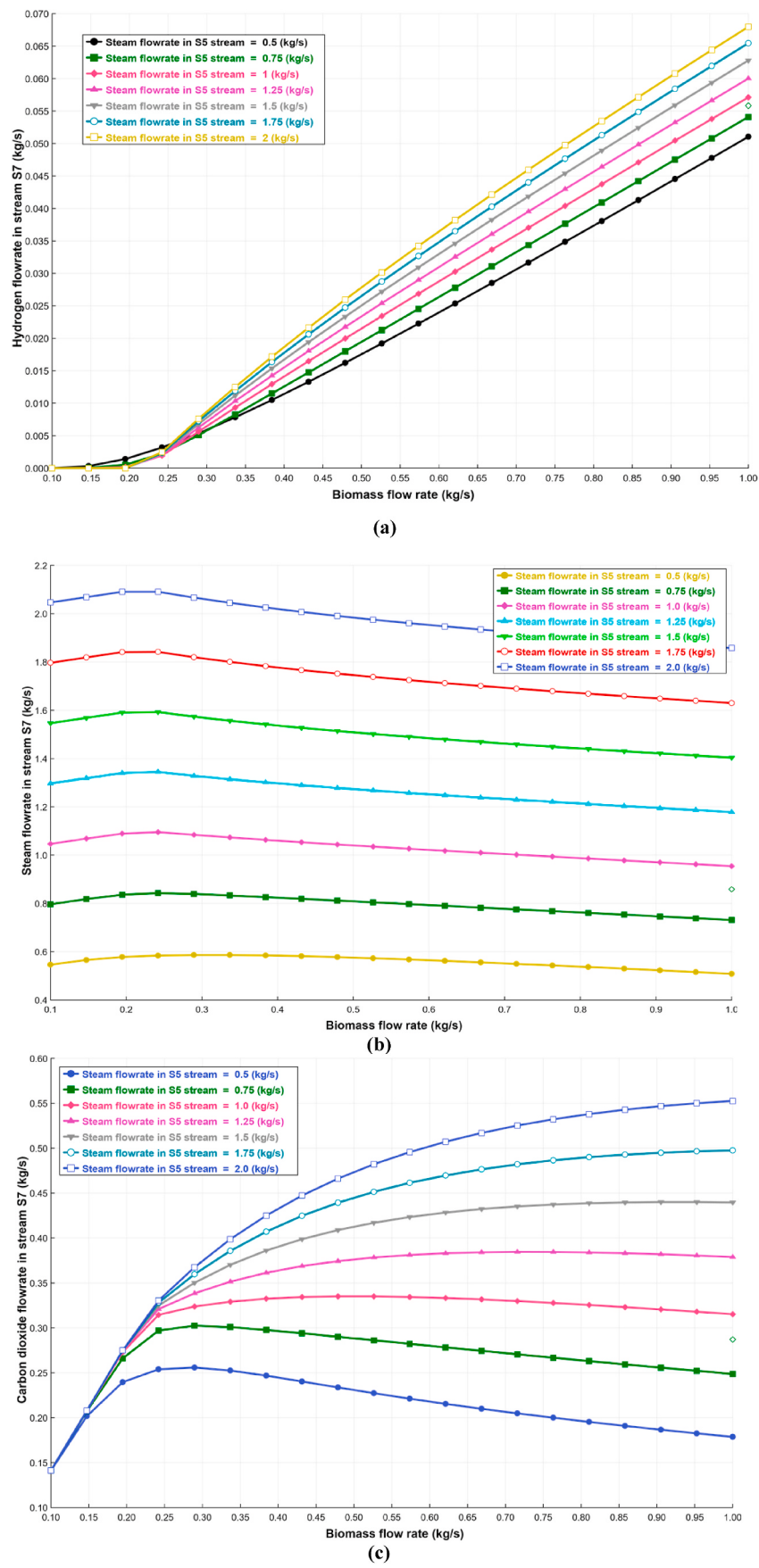


Fig. 7. (a) Effect of biomass and steam flow rate on hydrogen capacity, (b) Biomass and steam flow rate effect on the flowrate of steam and (c) Steam and biomass flowrate effect on carbon dioxide flowrate.

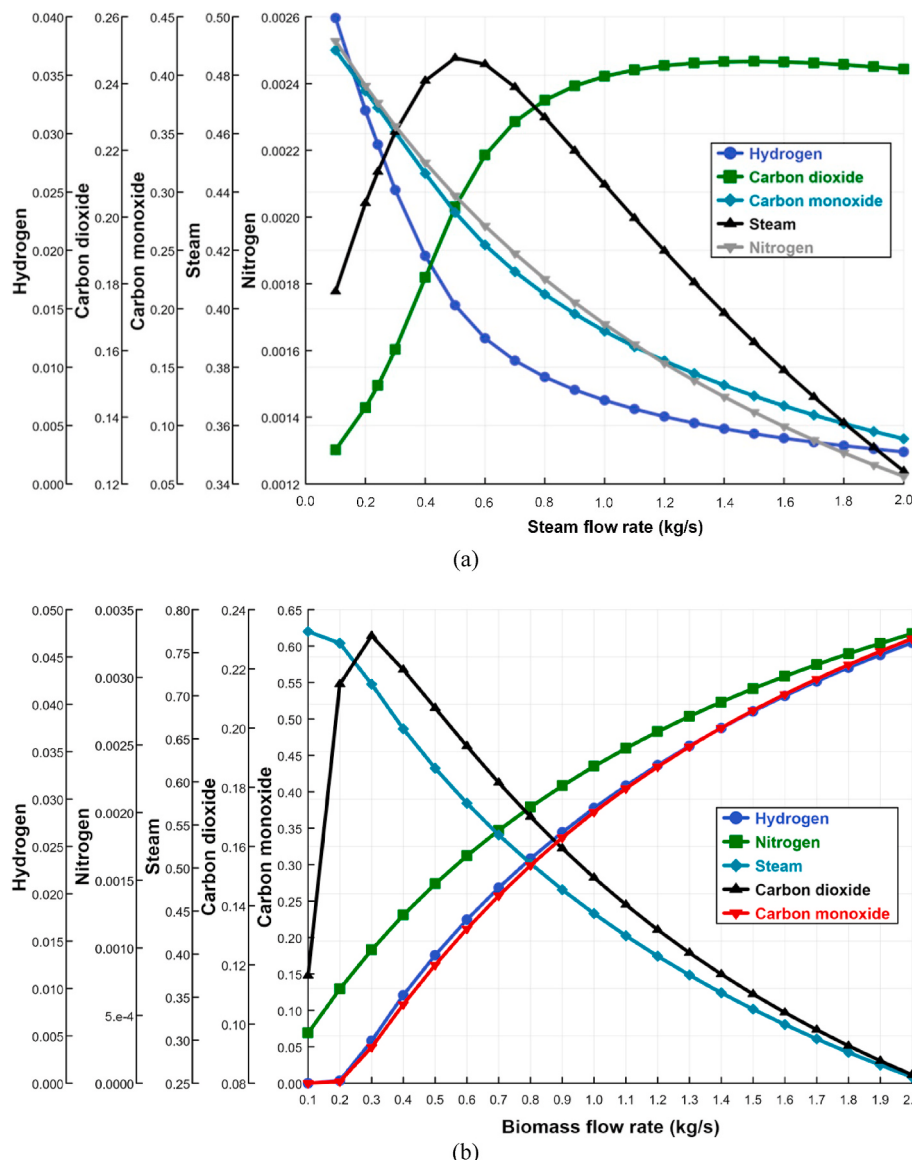


Fig. 8. Effect of biomass gasification parameters on mass fractions of each component (a) Steam flow rate effect (b) Biomass flowrate effect.

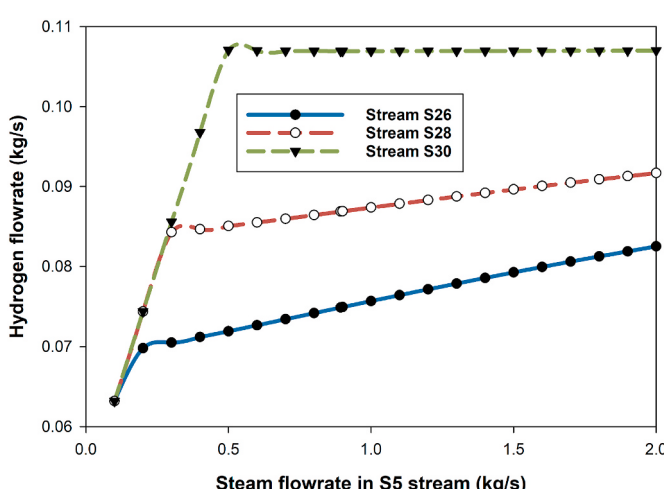


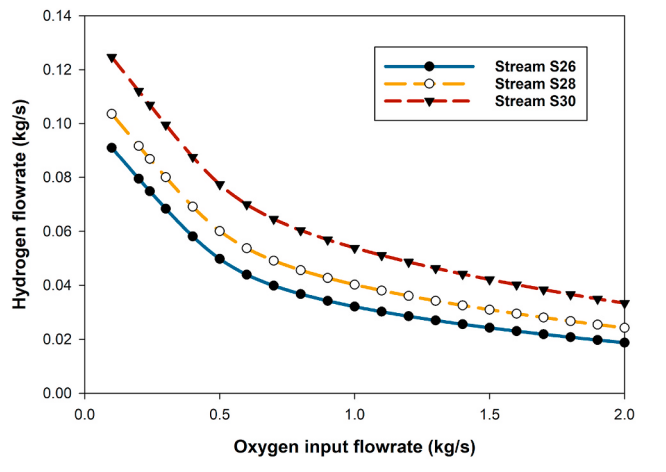
Fig. 9. Steam flow rate effect on the hydrogen capacities.

4.3. Parametric studies and sensitivity analyses for geothermal power generation based system

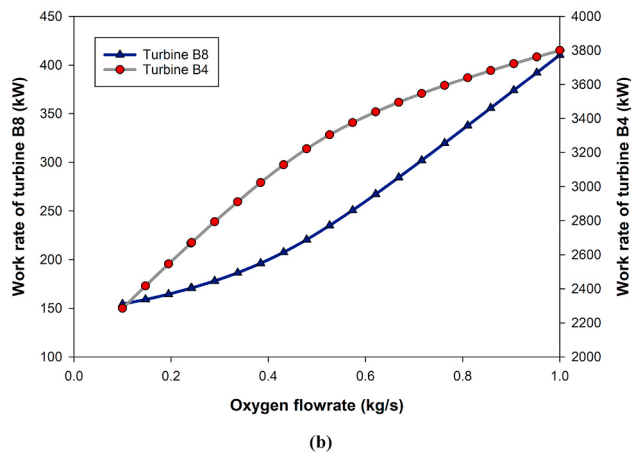
Hydrogen production using geothermal power is substantial to be investigated the system in terms of water temperature and pressure from the production well, flashing temperature and pressure, turbine efficiency, hydrogen production and system efficiencies. Turbine efficiency is assumed to be 80% and this study is important to investigate the turbine efficiency against turbine power and exergy destruction rate.

Fig. 11 displays the effect of the geothermal fluid flowrate on turbine power and hydrogen production. The significance of this study is to investigate the system under different operating parameters and to explore the scale-up options for the designed system. The geothermal fluid flowrate is considered in the range of 30–150 kg/s. The system is designed in a way that the electric power obtained from the turbine is directly fed to the PEM electrolyser. Figure shows that a rise in the geothermal fluid flowrate cause increase in turbine power and higher electric power results in increased hydrogen production.

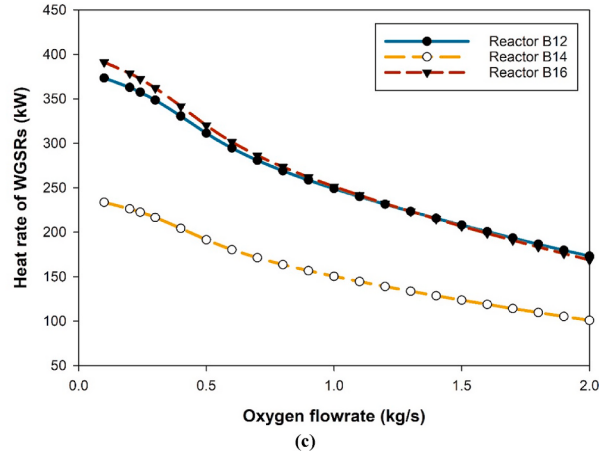
It is significant to explore the effect of turbine isentropic efficiency on the performance of the turbine in terms of turbine work and exergy destruction rates. **Fig. 12** shows the effect of turbine isentropic efficiency



(a)



(b)



(c)

Fig. 10. (a) Effect of oxygen input flow rate on the hydrogen production flowrates, (b) Oxygen flowrate effect on the work rate generated by the turbines and (c) Effect of oxygen flowrate on the heat duty of water gas shift reactors.

on the turbine power and exergy destruction rate. The range of turbine efficiency is taken from 70 to 90%. It can be depicted that an increase in turbine efficiency rises turbine power and reduces the exergy destruction.

Fig. 13(a) and (b) display the effect of turbine isentropic efficiency and flashing pressure on the overall energy and exergy efficiencies. The significance of these parametric studies is to investigate the performance index in terms of energy and exergy efficiencies under different operating conditions. Fig. 12(b) displays the effect of turbine isentropic

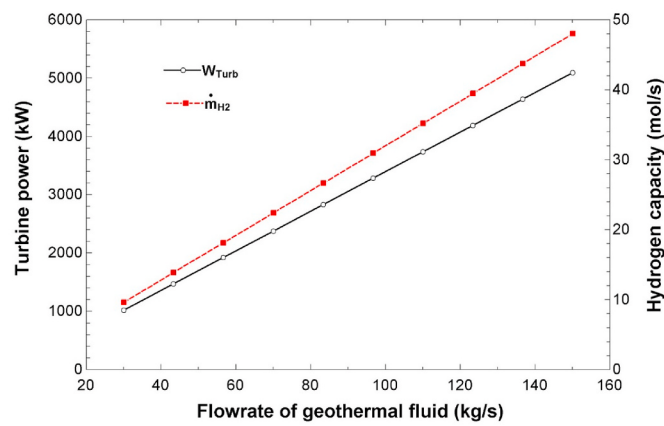


Fig. 11. Geothermal fluid flowrate effect on the turbine power and hydrogen capacity.

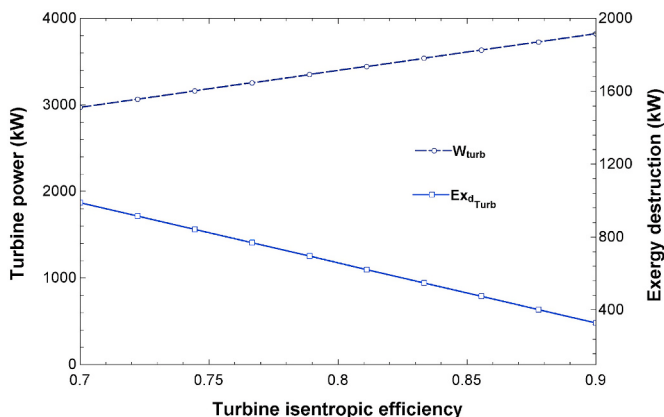


Fig. 12. Effect of turbine isentropic efficiency on the work and exergy destruction rate of turbine.

efficiency on the overall energetic and exergetic efficiencies and Fig. 12 (a) exhibits the effect of flashing pressure on the efficiencies. The range of the turbine isentropic efficiency is taken from 70 to 90% and flashing pressure is taken in the range of 400–800 kPa. It can be depicted that both, turbine isentropic efficiency and flashing pressure effects positively on the system performance and causes the energy and exergy efficiencies to increase gradually.

The effect of the flashing pressure is investigated against the turbine work rate, exergy destruction rates of turbine and flash chamber and flash temperature in Fig. 14(b). The hot geothermal fluid passes through a flash chamber which converts saturated liquid into the saturated mixture and produces vapor. This vapor stream then passes through the turbine to generate electricity. The flashing pressure is taken in the range of 400–800 kPa. It can be depicted that increase in flashing pressure causes turbine power to increase, exergy destruction rate of the turbine increases slightly, exergy destruction rate of the flash chamber decreases and flash temperature increases significantly from 140 to 170 °C, respectively.

5. Conclusions

This study develops three different configurations for renewable energy-based hydrogen production methods including solar PV, biomass gasification and geothermal power generation. All three systems are analysed thermodynamically in terms of energetic and exergetic approaches. Aspen Plus industrial software and EES are software tools employed for modeling purposes. This study also proposes a new

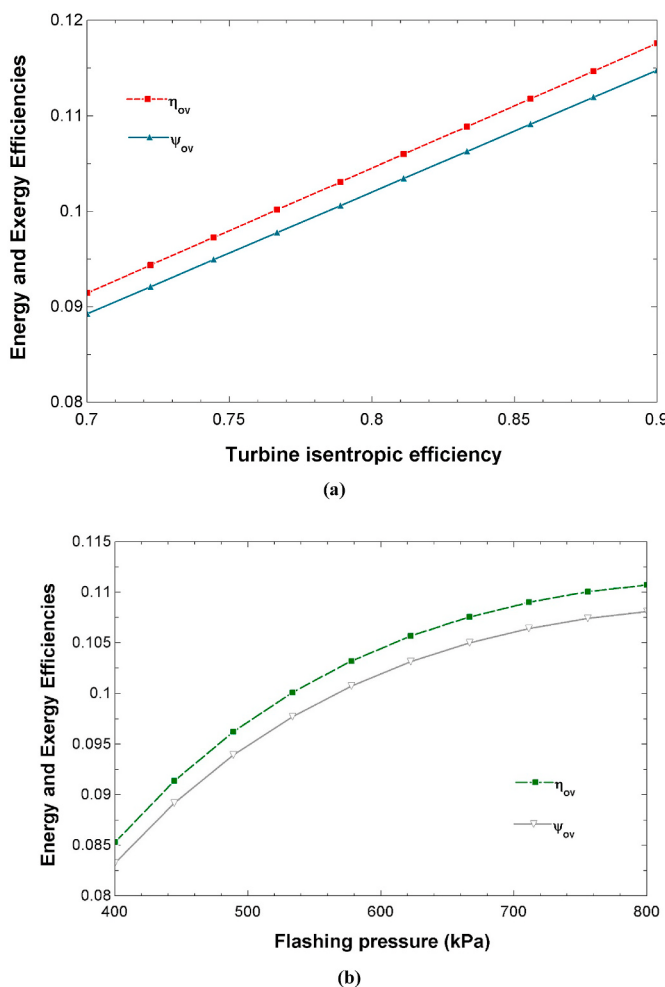


Fig. 13. (a) Effect of isentropic efficiency of turbine on the overall energy and exergy efficiencies and (b) effect of flashing pressure on the overall energy and exergy efficiencies.

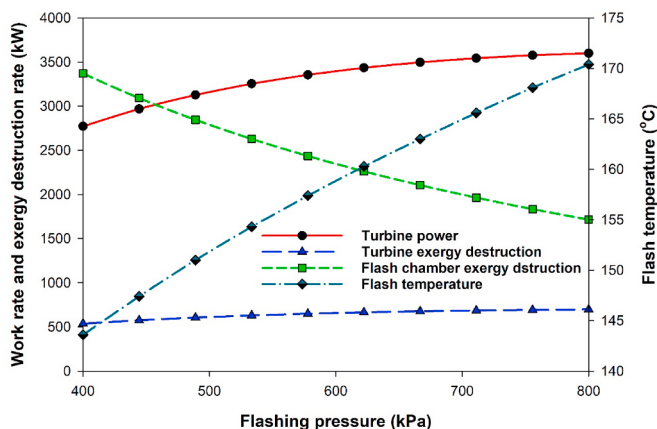


Fig. 14. Effect of the flashing pressure effect on the turbine power, exergy destructions of turbine and flash chamber and flash temperature.

approach of a multi-stage water gas shift reactor (MWGSR) which provides with the high conversion rate and converts CO in CO_2 by producing hydrogen. The performance index is measured in terms of energy and exergy efficiencies for all three systems and investigated under different operating conditions. It is recommended for future work to consider all conventional, renewable and hybrid type hydrogen

production methods under various source and operating conditions and types of units utilized. Some key findings of the study are summarized as follows:

- The overall energy and exergy efficiencies of the solar PV based hydrogen production system are 16.95% and 17.45% respectively and hydrogen production rate is found to be 2.26 g/s.
- The biomass gasification based hydrogen production system overcomes with the energy and exergy efficiencies of 53.6% and 49.8% with hydrogen production rate of 106.9 g/s.
- Geothermal energy based hydrogen production system is finalized with the energy and exergy efficiencies of 10.45% and 10.2% and system is capable of producing 32.02 g/s of hydrogen.

CRediT author contribution statement

H. Ishaq: Conceptualization, Methodology, Data curation, Contributed data or analysis tools, Formal analysis, Writing - original draft. **I. Dincer:** Writing - review & editing, Project administration, Validation, Supervision.

Declaration of competing interest

The authors declare that they have no known competing financial interests or personal relationships that could have appeared to influence the work reported in this paper.

References

- [1] Hosseini SE, Andwari AM, Wahid MA, Bagheri G. A review on green energy potentials in Iran. *Renew Sustain Energy Rev* 2013;27:533–45.
- [2] Moriarty P, Honnery D. What is the global potential for renewable energy? *Renew Sustain Energy Rev* 2012;16:244–52.
- [3] Chiari L, Zecca A. Constraints of fossil fuels depletion on global warming projections. *Energy Pol* 2011;39:5026–34.
- [4] Lund H. Renewable energy strategies for sustainable development. *Energy* 2007; 32:912–9.
- [5] Acar C, Dincer I. Review and evaluation of hydrogen production options for better environment. *J Clean Prod* 2019;218:835–49.
- [6] Dincer I, Acar C. Innovation in hydrogen production. *Int J Hydrogen Energy* 2017; 42:14843–64.
- [7] Collier K, Hahn D, Marion B. Solar hydrogen production demonstration. Conf Rec IEEE Photovolt Spec Conf 2002:635–9. <https://doi.org/10.1109/pvsc.1991.169288>.
- [8] Jeon HS, Min BK. Solar-hydrogen production by a monolithic photovoltaic-electrolytic cell. *J. Electrochem. Sci. Technol.* 2013;3:149–53.
- [9] Saadi A, Becherif M, Ramadhan HS. Hydrogen production horizon using solar energy in Biskra, Algeria. *Int J Hydrogen Energy* 2016;41:21899–912.
- [10] Hosseini SE, Wahid MA. Hydrogen production from renewable and sustainable energy resources: promising green energy carrier for clean development. *Renew Sustain Energy Rev* 2016;57:850–66.
- [11] Udomsirichakorn J, Salam PA. Review of hydrogen-enriched gas production from steam gasification of biomass: the prospect of CaO-based chemical looping gasification. *Renew Sustain Energy Rev* 2014;30:565–79.
- [12] Iribarren D, Susmoxas A, Petrakopoulou F, Dufour J. Environmental and energetic evaluation of hydrogen production via lignocellulosic biomass gasification. *J Clean Prod* 2014;69:165–75.
- [13] Nikolaidis P, Poullikkas A. A comparative overview of hydrogen production processes. *Renew Sustain Energy Rev* 2017;67:597–611.
- [14] Sikarwar VS, Zhao M, Clough P, Yao J, Zhong X, Memon MZ, Shah N, Anthony EJ, Fennell PS. An overview of advances in biomass gasification. *Energy Environ Sci* 2016;9:2939–77.
- [15] Muresan M, Cormos CC, Agachi PS. Techno-economical assessment of coal and biomass gasification-based hydrogen production supply chain system. *Chem Eng Res Des* 2013;91:1527–41.
- [16] Ud Din Z, Zainal ZA. Biomass integrated gasification-SOFC systems: technology overview. *Renew Sustain Energy Rev* 2016;53:1356–76.
- [17] Yilmaz C, Kanoglu M, Bolatturk A, Gadalla M. Economics of hydrogen production and liquefaction by geothermal energy. *Int J Hydrogen Energy* 2012;37:2058–69.
- [18] Missimer TM, Choon Ng K, Thuw K, Wakil Shahzad M. Geothermal electricity generation and desalination: an integrated process design to conserve latent heat with operational improvements. *Desalin. Water Treat.* 2016;57:23110–8.
- [19] Ozden E, Tari I. Energy-exergy and economic analyses of a hybrid solar-hydrogen renewable energy system in Ankara, Turkey 2016. <https://doi.org/10.1016/j.aplthermaleng.2016.01.042>.
- [20] Safarian S, Unnpörsson R, Richter C. A review of biomass gasification modelling. *Renew Sustain Energy Rev* 2019;110:378–91.

- [21] Wang F, Deng S, Zhao J, Wang J, Sun T, Yan J. Performance and economic assessments of integrating geothermal energy into coal-fired power plant with CO₂ capture. *Energy* 2017;119:278–87.
- [22] Channiwala SA, Parikh PP. A unified correlation for estimating HHV of solid, liquid and gaseous fuels. *Fuel* 2002;81:1051–63.
- [23] Wang H, Bai X, Ma G. Reliability assessment of grid-integrated solar photovoltaic system. *Power Syst Technol* 2012;36:1–5.
- [24] Ishaq H, Dincer I, Naterer GF. Performance investigation of an integrated wind energy system for co-generation of power and hydrogen. *Int J Hydrogen Energy* 2018;43:9153–64.
- [25] Carmo M, Fritz DL, Mergel J, Stolten D. A comprehensive review on PEM water electrolysis. *Int J Hydrogen Energy* 2013;38:4901–34.
- [26] Briguglio N, Antonucci V. Overview of PEM electrolysis for hydrogen production. PEM electrolysis hydrog. *Prod Princ Appl* 2015;389. <https://doi.org/10.1201/b19096-2>.
- [27] Kotowicz J, Sobolewski A, Iluk T. Energetic analysis of a system integrated with biomass gasification. *Energy* 2013;52:265–78.
- [28] Al-Zareer M, Dincer I, Rosen MA. Influence of selected gasification parameters on syngas composition from biomass gasification. *J Energy Resour Technol* 2018. <https://doi.org/10.1115/1.4039601>.
- [29] Khaliq A. Exergy analysis of gas turbine trigeneration system for combined production of power heat and refrigeration. *Int J Refrig* 2009;32:534–45.